Supplementary Material – Methodology

Electron probe microanalysis (EPMA)

Quantitative EPMA were obtained using a CAMECA SX-Five Electron Probe Microanalyzer (EPMA), equipped with 5 wavelength-dispersive spectrometers (Adelaide Microscopy, The University of Adelaide). The instrument was operated at a constant accelerating voltage of 15 keV and variable beam current (see below). A constant beam spot-size of ~1 μm was utilized for the measurements. Individual analytical conditions for each analyzed element are listed below. Calibration and data reduction were conducted using 'Probe for EPMA' software (Donovan et al. 2016).

<mdl: less than minimum limit of detection.

Element	Line	Current (nA)	Crystal	Standard	Peak count (s)	Bkgd count (s)	Mean mdl (wt%)
Al	Kα	20	TAP	Astimex Plagioclase An65	20	10	0.012
Ca	Kα	20	LPET	Titanite	20	10	0.011
Fe	Kα	20	LLIF	P&H Specularite	20	10	0.03
Mg	Kα	100	TAP	Astimex Almandine	50	25	0.004
Mn	Kα	20	LLIF	P&H Rhodonite	20	10	0.028
Si	Kα	20	TAP	Astimex Plagioclase An65	20	10	0.013
Ti	Kα	20	LPET	Titanite	50	25	0.008
V	Kα	100	LLIF	Astimex Vanadium metal	35	20	0.007
Zn	Kα	100	LLIF	Astimex Willemite	50	25	0.019

Laser ablation inductively coupled plasma mass spectrometry (LA-ICP-MS)

^{57}Fe was used as the internal standard element, assuming a stoichiometric Fe content in magnetite. External reference materials GSD-1G and NIST-610 were used for trace element quantification and instrument drift correction. A laser spot diameter of 43 or 51 μm, pulse repetition rate of 5 Hz and fluence of 3.5 J/cm^2 were used. Data reduction was performed in Glitter (van Achterbergh et al. 2001). Analysis comprised 44 elements by measurement of the following isotopes: ^{24}Mg, ^{27}Al, ^{28}Si, ^{31}P, ^{43}Ca, ^{45}Sc, ^{49}Ti, ^{51}V, ^{52}Cr, ^{55}Mn, ^{59}Co, ^{60}Ni, ^{63}Cu, ^{66}Zn, ^{69}Ga, ^{75}As, ^{88}Sr, ^{89}Y, ^{90}Zr, ^{93}Nb, ^{95}Mo, ^{118}Sn, ^{121}Sb, ^{137}Ba, ^{139}La, ^{140}Ce, ^{141}Pr, ^{146}Nd, ^{147}Sm, ^{153}Eu, ^{157}Gd, ^{159}Tb, ^{163}Dy, ^{165}Ho, ^{166}Er, ^{169}Tm, ^{172}Yb, ^{175}Lu, ^{178}Hf, ^{181}Ta, ^{182}W, ^{232}Th, ^{238}U, and four isotopes of lead (^{204}Pb, ^{206}Pb, ^{207}Pb and ^{208}Pb).

Supplementary Material – Additional figures

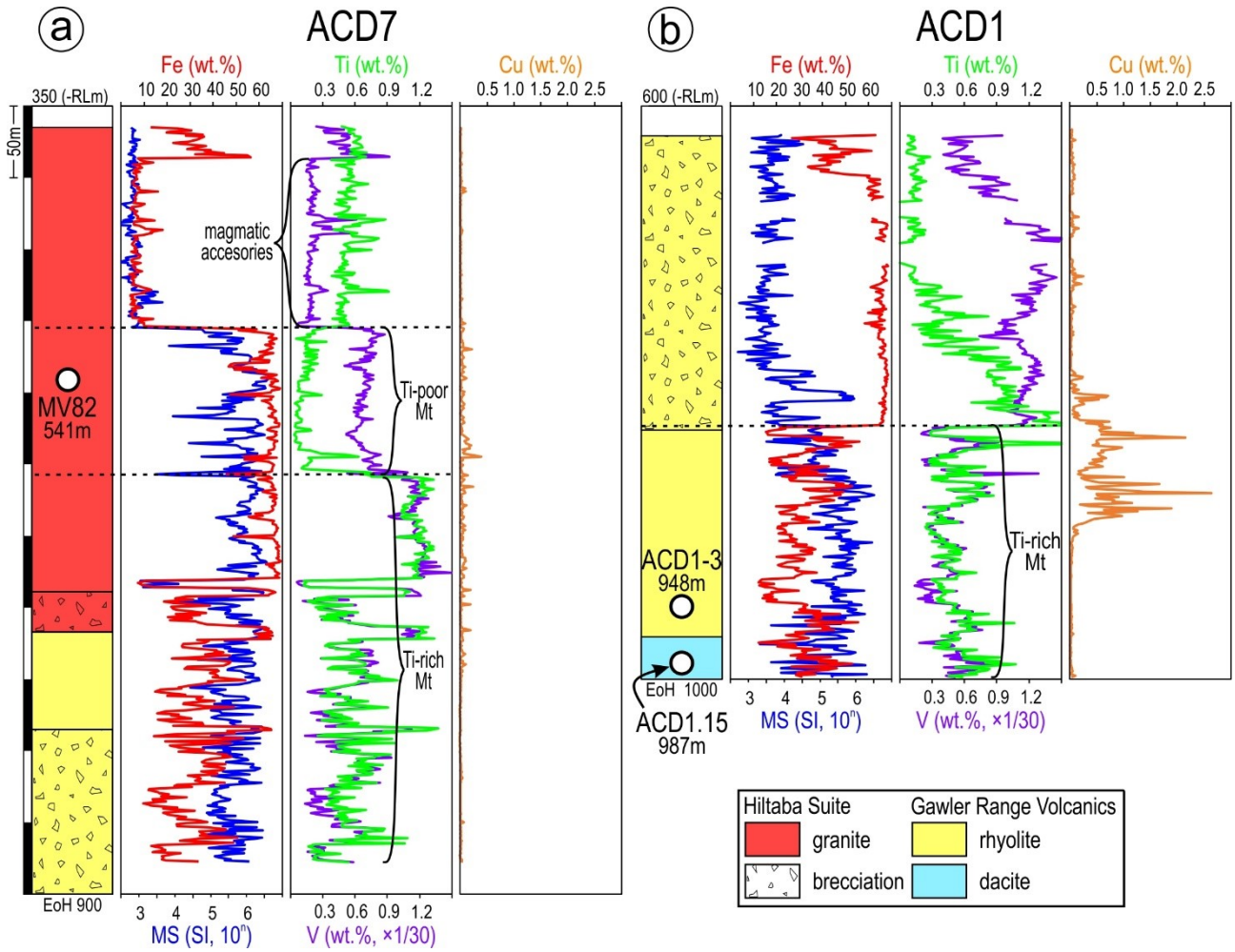

Fig. A1. (a, b) Schematic drillhole logs for holes ACD7 and ACD1, respectively, showing sample locations, simplified lithologies and downhole distributions of Ti, V, and Cu, relative to Fe and magnetic susceptibility (MS; standard international-SI). Whole-rock assays are at 1-meter intervals. Note the good spatial correlation between V and Ti relative to increases in Fe and MS associated with magnetite-rich intervals. Divergences between measured Fe contents and MS relate to the presence of hematite. High Ti-contents in the upper part of drillhole ACD7 relate to the presence of Ti-bearing magmatic accessories. Abbreviation: Mt−magnetite. Iron-oxides are present within cm-wide veins that are locally interconnected (stockwork, patches and disseminations).

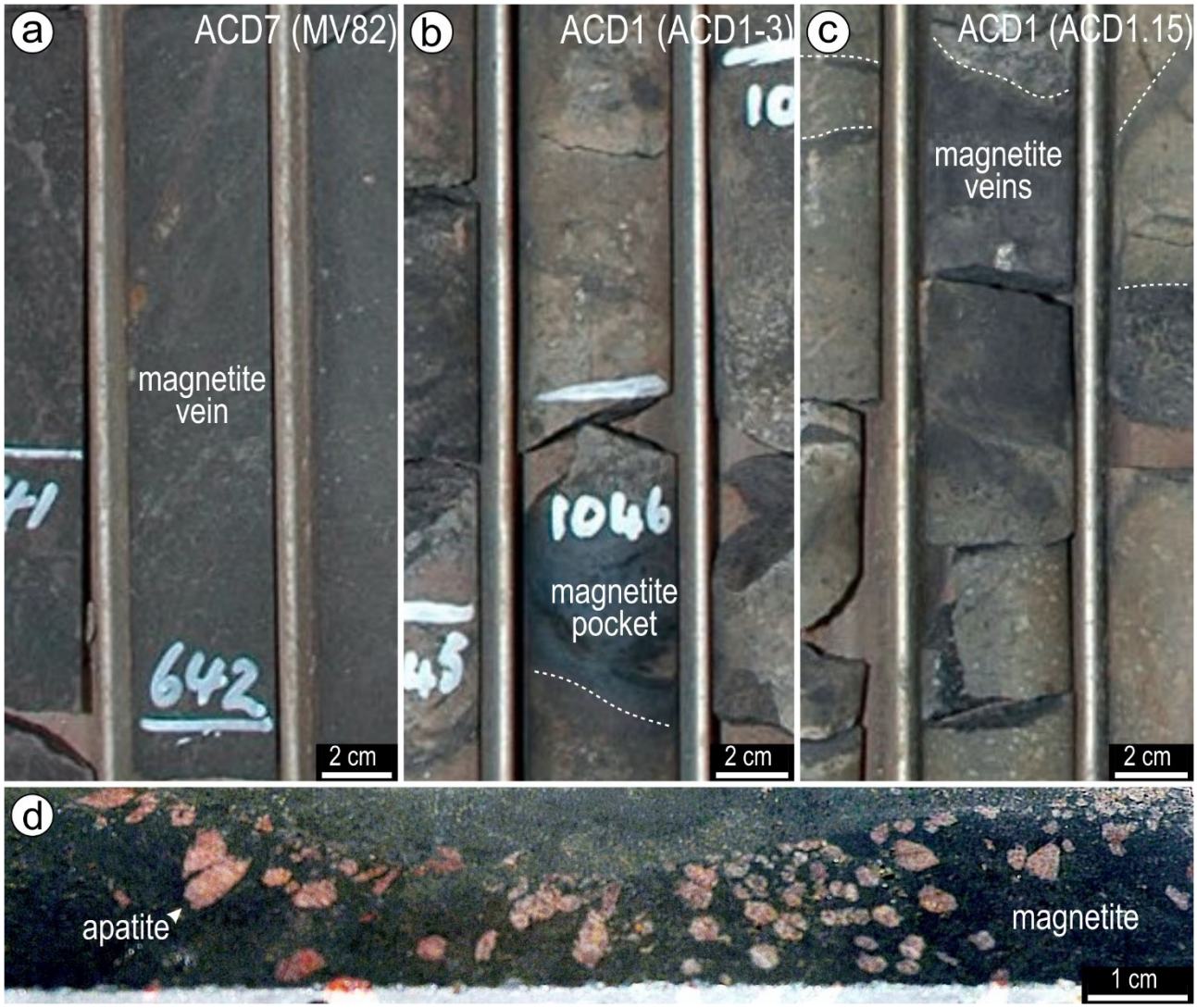

Fig. A2. Photographs of Acropolis drillcore showing sampled sections. (a) Vein of massive magnetite sectioned along dip within Hiltaba Suite (HS) granite (drillhole ACD7; sample MV82). (b, c) Magnetite-rich intervals hosted within altered Gawler Range Volcanics (GRV) lithologies from drillhole ACD1; in (b) rhyolite (sample ACD1-3) and (c) dacite (sample ACD1.15). (d) Interstitial apatite grains within magnetite vein in HS granite (drillhole ACD7).

Supplementary Material – Petrographic background for nanoscale study

In two samples (samples MV82 and ACD1.15), magnetite is coarse-grained (~300 μm-diameter), relatively equigranular, and represents >90 % of the polished block. In the third sample (ACD1-3 SK), magnetite occurs as veinlets within a groundmass of altered rhyolite.

The uppermost ~100 m-thick segment of granite partially preserves magmatic Fe-Ti-oxides, albeit with strong martitization of magnetite and replacement of titanite(+ilmenite?) by symplectites consisting of rutile, secondary silicates and carbonates (Fig. A3a). Symplectitic intergrowths among Fe-Ti-oxides, filling discrete grains in titanomagnetite from the same drillhole, ACD7, are attributable to breakdown of ilmenite$_{ss}$ within Ti-bearinghematite (Fig. A3b). Two S/TEM foils were prepared from the Ti-poor magnetite hosted in granite (Fig. A3c, d). This magnetite displays thin, ~10 μm-wide hematite veinlets (Fig. A3e). Up to ~15 % hematite is estimated within this sample (MV82).

Trellis magnetite hosted in GRV was sampled from the deeper part of drillhole ACD1 (sample ACD1.15; Fig. A4). In this case, veinlets filled with Fe-Ti-oxides, Ti-bearing hematite and secondary Fe-hydroxides (+carbonates and quartz) are also observed and display boxwork textures typical of supergene/fault gouge alteration (Fig. A4a, b). The S/TEM foil was obtained from the margin of a grain adjacent to hematite zoned with respect to Ti and also contains nanoscale inclusions of ilmenite and rutile (Fig. A4c, d).

A second type of trellis Ti-rich magnetite, displaying various overprinting textures, was studied from the upper interval of the same drillhole (sample ACD1-3 SK; Fig. A5). Coarser, mm-sized magnetite occurs along a vein of baryte (Fig. A5a-c). The magnetite is otherwise fine-grained and brecciated to partially milled. One of the two textural varieties consist of magnetite densely mottled with inclusions, whereby the trellis networks are partially obliterated towards the grain margin (Fig. A5d). The second type displays orbicular textures developed within and across some of the lamellae forming the trellis frameworks (Fig. A5e). Three S/TEM foils were obtained from the margin of a densely mottled grain and two from the orbicular patterned grain (Fig. A5f, g).

Diverse textures relate to the martitization of Ti-rich magnetite (hosted by either HS granite or GRV rocks) towards the upper part of each drillhole (Fig. A6). Marginal martitization evolves into wider embayed domains where hematite replaces Ti-rich magnetite (Fig. A6a, b). In such cases the trellis network is still partially visible within the hematite aggregate at the direct contact with magnetite, but is partly obliterated in the patchy, outwards-growing aggregates of hematite (Fig. A6b). The occurrence of fine-grained symplectitic intergrowths of Fe-Ti-oxides surrounded by Ti-rich hematite (Fig. A6c) is typical of Ti-rich magnetite undergoing martitization. Such intergrowths are ubiquitous throughout the Ti-rich magnetite in the prospect but decrease in abundance towards the upper part of each drillhole. Recrystallization of such Ti-rich oxide aggregates results in coarser grained rutile and Ti-zoned hematite forming aggregates within pockets or along veinlets throughout the Ti-rich magnetite (Fig. A6d-f). Development of lamellar to acicular Ti-bearing hematite along some of the veinlets affected by supergene/fault gouge alteration results in typical boxwork textures host to secondary Fe-hydroxides, siderite and quartz (Fig. A6g).

Although hematite inherits a Ti-signature from magnetite during martitization, this changes to U-W-Sn-Mo in martite in the uppermost part of some drillholes, e.g., ACD2 (Courtney-Davies et al. 2019a; Fig. A6h). Some of the Ti-(Fe)-oxides forming parts of Ti-zoned hematite may be attributed to the breakdown of ilmenite$_{ss}$ within Ti-bearing hematite. Formation of later hematite can be accompanied

by replacement of magnetite by bornite (Fig. A6i). In this case, hematite appears as stubby lamellae associated with covellite. The presence of covellite and hematite (and lack of Fe-hydroxides) may indicate highly acidic and oxidized fluids for sulfide precipitation prior to martite formation.

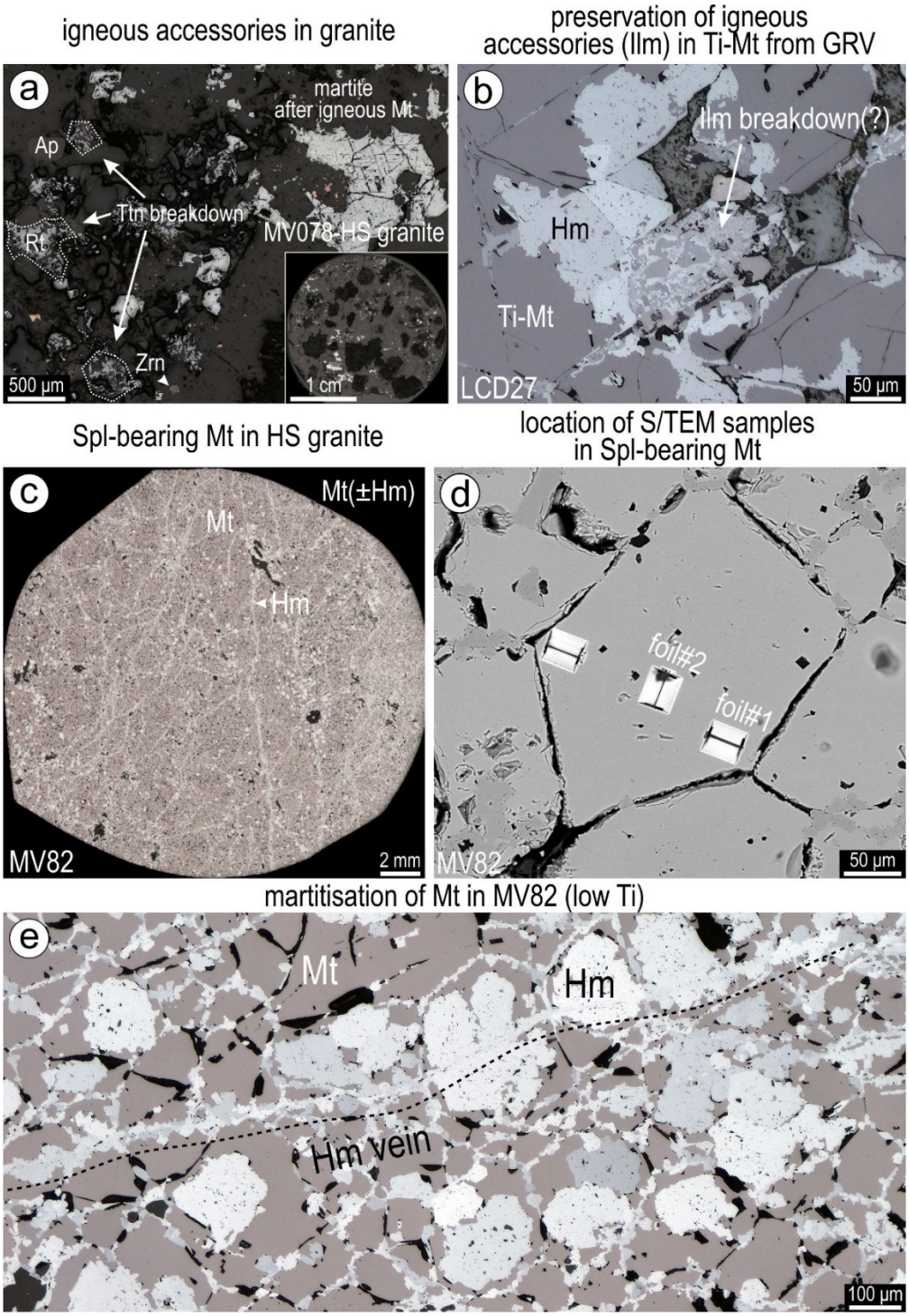

Fig. A3. Reflected light photographs (a-c, e) and BSE image (d) showing petrographic aspects of Fe-oxides in samples from drillhole ACD7. (a) Magmatic accessories in HS granite. (b) Fine-grained symplectites of rutite+hematite interpreted as breakdown ilmenite in volcanic rock (GRV). (c, d) Map of polished block in (c) and location of S/TEM samples in (d) from the magnetite with nanoinclusions of spinel. (e) Martitization of magnetite shown in (c). Abbreviations: Ap−apatite; Hm−hematite; Ilm−ilmenite; Mt−magnetite; Rt−rutile; Spl−spinel; Ttn−titanite; Ti-Mt−titanomagnetite; Zrc−zircon. Additional samples in drillhole ACD7 and RL depth: MV078, 366 m; LCD27, 878 m.

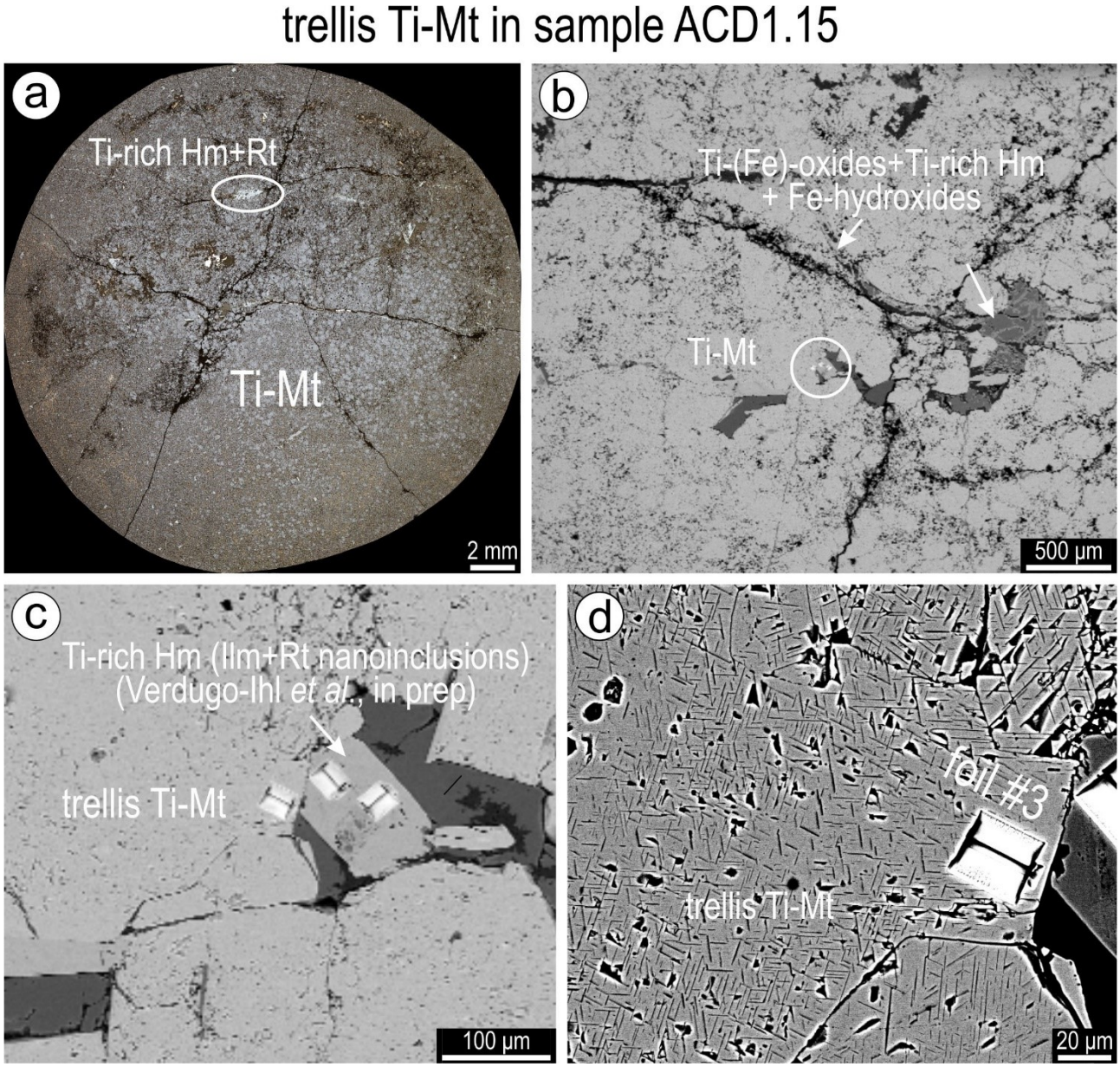

Fig. A4. Reflected light photograph (a) and BSE images (b-d) of trellis titanomagnetite. (a) Map of polished block of titanomagnetite. (b) Area of sample in (a) with fractures and pockets of Fe-Ti-oxides and Fe-hydroxides (arrowed). (c) Close up of the area circled in (b) showing typical trellis titanomagnetite adjacent to a coarse grain of Ti-rich hematite. (d) Location of S/TEM sample across trellis lamellae (Ti-rich). Abbreviations: Hm−hematite; Ilm−ilmenite; Ti-Mt−titanomagnetite; Rt−rutile.

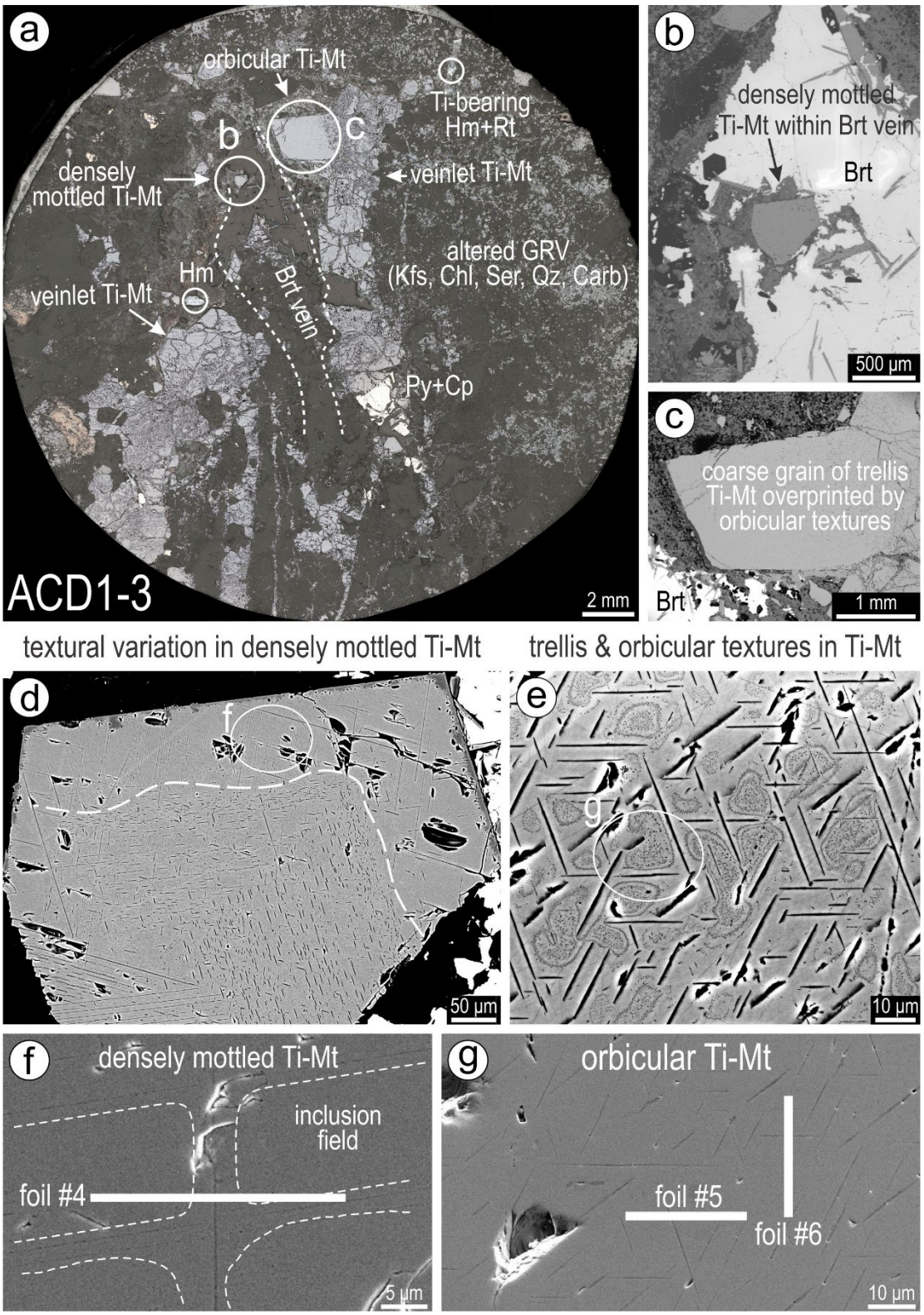

Fig. A5. Reflected light photograph (a) and BSE images (b-g) showing petrographic aspects of trellis titanomagnetite with overprint. (a) Map of polished block of veinlets of titanomagnetite in altered volcanic rock. (b, c) Details of the two magnetite grains that were sampled for nanoscale study. (d) Grain of titanomagnetite with margin depleted in trellis lamellae (dashed line) and enriched in densely mottled nanoinclusions. (e) Detail of trellis titanomagnetite with orbicular texture. (f, g) Location of S/TEM samples obtained from the two magnetite grains obtained from the circled areas marked in (d, e). Abbreviations: Brt−barite; Carb−carbonates; Chl−chlorite; Cp−chalcopyrite; Hm−hematite; Kfs−potassium feldspar; Py−pyrite; Qz−quartz; Ti-Mt−titanomagnetite; Rt−rutile; Ser−sericite.

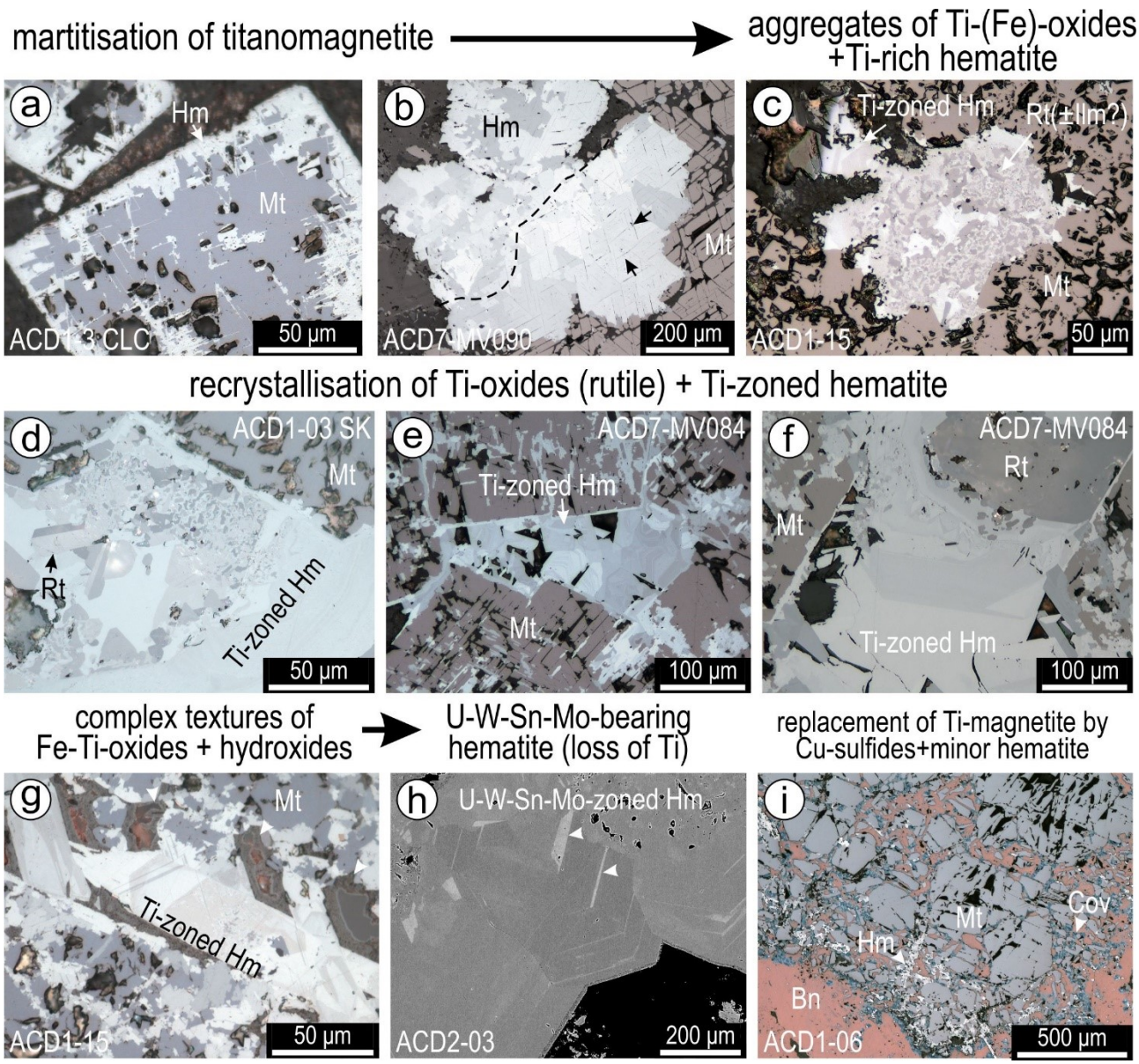

Fig. A6. Reflected light photographs showing titanomagnetite martitization (a-h) and replacement by Cu-sulfides in (i). (a) Martitization along grain boundary. (b) Coarse aggregate of hematite partially preserving trellis lamellae (dashed line). Fine-grained aggregates of Ti-(Fe)-oxides and hematite within titanomagnetite. (d-f) Titanium-bearing/rich zoned hematite associated with rutile resulting from recrystallisation as shown in (c). (g) Iron-hydroxides with rhythmic-orbicular textures typical of gauge-fault alteration surrounding Ti-zoned hematite. (h) U-W-Sn-Mo-zoned hematite that was dated at ~1.6 Ga (U-Pb LA-ICP-MS; Courtney-Davies et al. 2019). Arrows show some of the highest U-bearing bands. (i) Bornite replacing magnetite. Note the presence of covellite and hematite throughout the replaced magnetite. Abbreviations: Bn−bornite; Cov−covellite; Hm−hematite; Ilm−ilmenite; Mt−magnetite; Rt−rutile. Additional samples location and RL depth: Drillhole ACD1: ACD1-3CLC: 806.8 m; ACD1-06: 866.6 m; Drillhole ACD7: MV084: 619 m; MV090: 810 m.

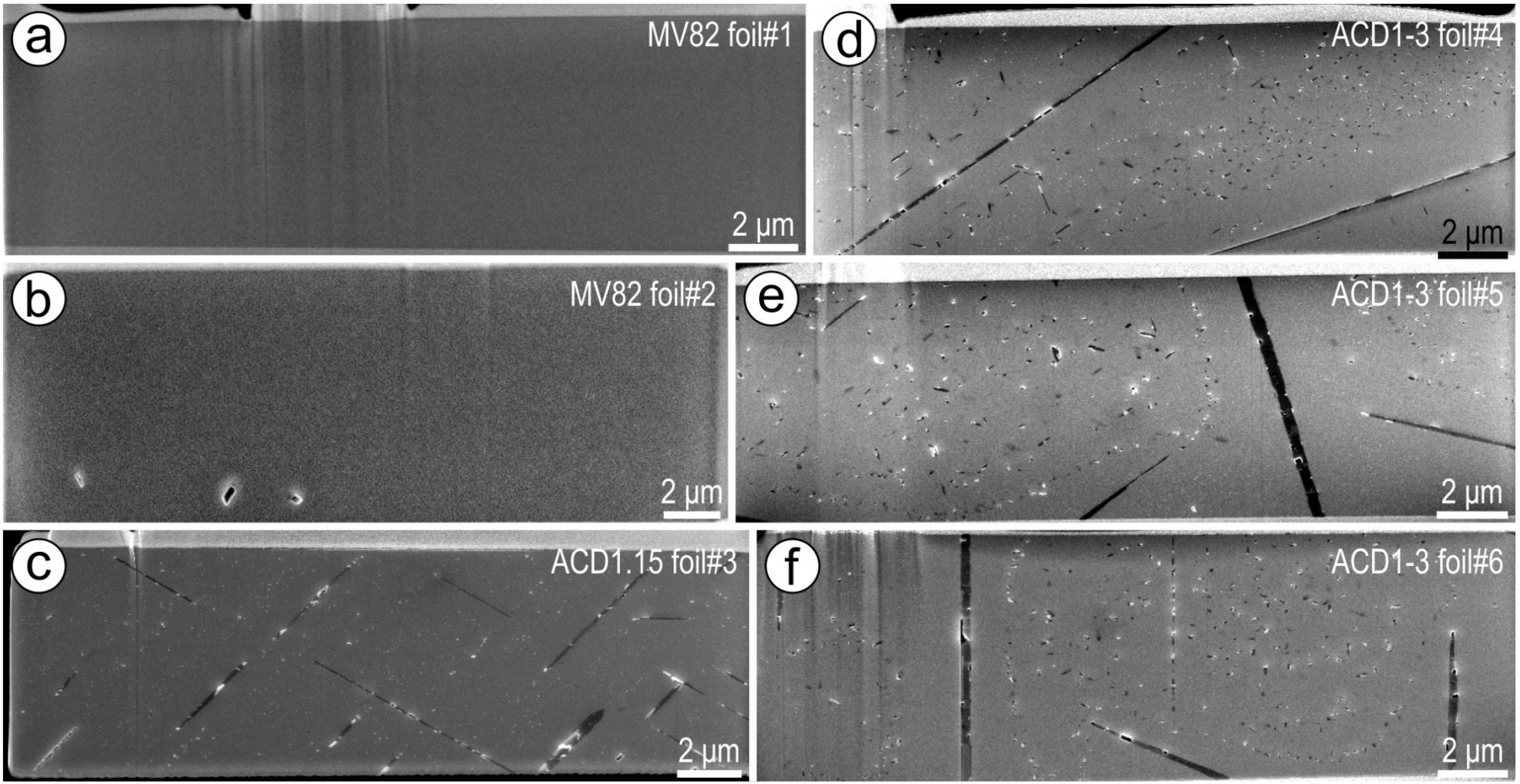

Fig. A5. SE images of the six FIB- extracted slices (#1-#6) prior to thinning and cleaning. (a, b) Titanium-poor magnetite; (d-f) Ti-rich magnetite: (c) trellis-textured magnetite, (d) densely mottled magnetite, and (e, f) orbicular magnetite.

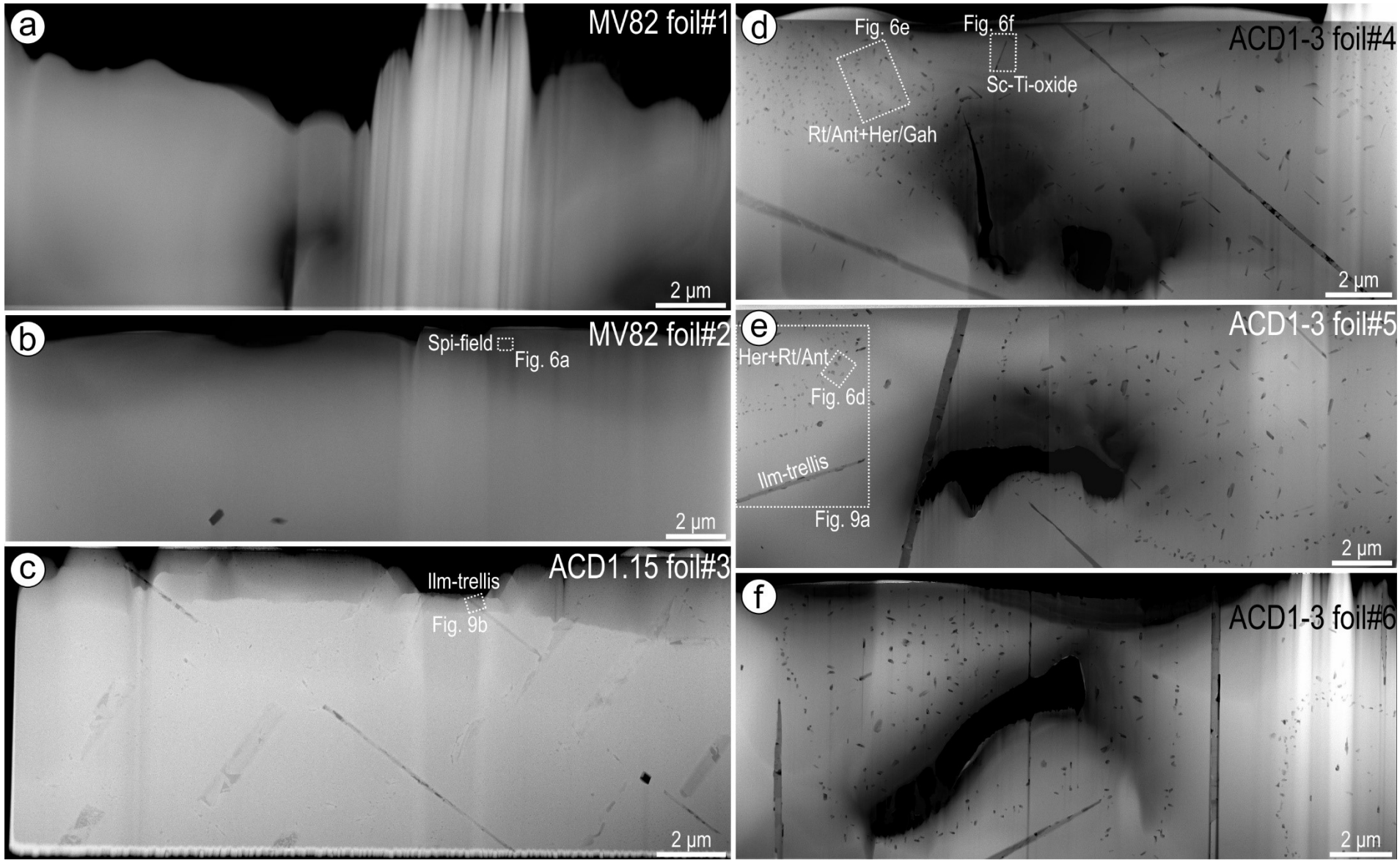

Fig. A6. (a-f) High angle annular dark field (HAADF) scanning transmission electron microscopy (STEM) images showing location of STEM-EDX maps of lamellae and/or associated inclusion fields. Abbreviations: Ant−anatase; Gah−gahnite; Her−hercynite; Ilm−ilmenite; Rt−rutile; Spi−spinel.

Supplementary Materials – Additional tables

Table A1. Summary of magnetite compositions as determined by EPMA and mineral formulae

Sample	Ti-rich magnetite									Ti-poor magnetite		
	trellis (ACD1.15, *n*=5)			orbicular (ACD1-3, *n*=9)			orbicular, ilm (ACD1-3, *n*=7)			(MV82, *n*=15)		
Concentration, wt%	Min.	Max.	Mean	Min.	Max.	Mean	Min.	Max.	Mean	Min.	Max.	Mean
CaO	0.02	0.03	0.03		<0.02			<0.02		<0.02	0.03	0.00
MgO		<0.01		<0.04	0.25	0.14	0.54	1.62	0.80	0.26	0.54	0.45
TiO_2	0.62	3.09	1.75	0.27	1.70	0.75	4.27	12.72	6.52	0.03	0.07	0.05
SiO_2	<0.02	0.06	0.04	0.03	0.06	0.05	0.03	0.06	0.05	0.03	0.11	0.05
Al_2O_3	0.32	0.39	0.36	0.32	0.54	0.44	0.38	0.76	0.54	0.23	0.33	0.29
$Fe_2O_{3(Total)}$	99.36	102.71	100.93	101.14	105.35	103.82	88.34	99.65	97.03	101.61	104.36	102.83
FeO	31.61	33.79	32.57	31.56	32.94	32.16	34.17	38.68	35.80	30.07	31.23	30.54
Fe_2O_3	61.98	67.44	64.73	65.43	69.63	68.08	45.35	61.67	57.24	68.20	69.65	68.89
MnO		<0.02		<0.05	0.08	0.02	<0.05	2.20	0.76	<0.05	0.13	0.07
ZnO	0.03	0.04	0.04	<0.06	0.10	0.01		<0.06			<0.06	
V_2O_3	0.05	0.07	0.06	<0.05	0.09	0.06	<0.06	0.09	0.02		<0.05	
Sum	99.04	100.28	99.57	99.24	103.11	101.70	100.17	102.73	101.73	99.27	101.57	100.34
Calculated formulae (atoms per formula unit; apfu) based on 32 O atoms												
Mg	0.000	0.000	0.000	0.000	0.111	0.062	0.240	0.716	0.354	0.117	0.249	0.204
Ca	0.006	0.010	0.008	0.000	0.000	0.000	0.000	0.000	0.000	0.000	0.011	0.001
Mn	0.000	0.000	0.000	0.000	0.019	0.004	0.000	0.551	0.190	0.000	0.034	0.017
Fe^{2+}	8.137	8.715	8.401	7.996	8.404	8.118	8.560	9.577	8.931	7.760	7.904	7.806
Zn	0.007	0.009	0.008	0.000	0.021	0.002	0.000	0.000	0.000	0.000	0.000	0.000
$\sum M^{2+}$			8.417			8.185			9.475			8.028
Al	0.115	0.142	0.130	0.114	0.197	0.156	0.136	0.267	0.189	0.083	0.117	0.103
V	0.014	0.017	0.015	0.000	0.022	0.015	0.000	0.022	0.005	0.000	0.000	0.000
Fe^{3+}	14.385	15.561	15.020	15.022	15.717	15.458	10.103	13.902	12.856	15.807	15.864	15.841
$\sum M^{3+}$			15.165			15.629			13.050			15.944
Si	0.000	0.018	0.011	0.010	0.018	0.014	0.010	0.017	0.013	0.009	0.035	0.017
Ti	0.142	0.718	0.406	0.062	0.391	0.172	0.963	2.832	1.462	0.008	0.016	0.011
$\sum M^{4+}$			0.417			0.185	0.974	2.844	1.475	0.019	0.046	0.028
Sum			24			24			24			24
X_{Mg}	-	-	-	0.0019	0.0047	0.0029	-	-	-	0.0049	0.010	0.0086
Temperature, °C	-	-	-	531	608	565	-	-	-	613	690	667

Sample means calculated considering values below minimum detection limits as zero. Blanks denote that all measurements within a sample were below minimum detection limits. Temperature estimates calculated using the empirical thermometer of Canil and Lacourse (2020). Abbreviations: Min.−minimum; Max.−maximum.

Table A2. Summary statistics of magnetite trace element data by LA-ICP-MS, concentrations in ppm.

Type	Ti-rich magnetite										Ti-poor magnetite				
variety/	trellis (ACD1.15, *n*=37)					orbicular (ACD1-3, *n*=30)					(MV82, *n*=21)				
sample	Min.	Max.	Mean	G.M.	S.D.	Min.	Max.	Mean	G.M.	S.D.	Min.	Max.	Mean	G.M.	S.D.
Mg	48.5	1,450	404	242	424	18.9	1,480	341	216	343	1,150	3,250	2,130	2,050	612
Al	1,610	3,910	2,610	2,570	450	1,910	2,560	2,230	2,230	176	1,440	1,560	1,490	1,490	27.8
Si	518	4,750	1,520	1,270	1,020	63.9	492	164	154	71.2	224	687	318	306	103
P	<28.9	186	58.3	50.8	35.6	<2.46	12.2	5.84	5.12	3.04	<2.7	25.3	13.9	12.3	6.45
Ca	NA	NA	NA	NA	NA	<16.5	49.3	22.8	21.8	8.09	<23.6	79.7	36.6	34.0	16.2
Sc	11.4	36.6	24.6	23.6	7.12	27.1	44.7	37.2	36.9	4.22	4.46	5.05	4.77	4.77	0.12
Ti	6,700	16,400	12,800	12,600	2,180	9,600	14,700	11,200	11,200	1,230	371	419	399	399	13.3
V	356	473	414	413	29.1	419	479	442	442	16.6	230	249	235	235	4.35
Cr	<0.77	7.06	2.83	2.63	1.12	<0.17	67.1	5.91	1.54	12.5	<0.19	1.10	0.29	0.25	0.21
Mn	32.9	118	58.3	56.5	15.8	48.3	534	126	99.2	111	155	681	343	312	150
Co	14.9	26.5	20.1	20.0	2.42	26.6	42.0	31.2	31	3.77	116	128	121	121	3.16
Ni	24.6	50.6	34.7	34.1	6.49	29.9	43.2	34.8	34.7	2.84	59.7	65.0	61.8	61.8	1.33
Cu	<0.92	39.4	7.46	4.27	8.52	<0.076	1.77	0.22	0.15	0.32	0.88	3.1	1.61	1.52	0.58
Zn	64.1	267	188	179	53.3	72.7	400	134	120	73.3	63.8	77.1	69.9	69.8	3.76
Ga	31.4	52.9	40.7	40.4	5.09	42.3	57.1	48.9	48.8	4.06	14.5	16.2	15.2	15.2	0.40
As	<0.81	3.99	2.16	1.93	1.01	<0.13	0.64	0.22	0.20	0.11	<0.16	0.35	0.20	0.20	0.047
Sr	0.054	10.8	3.01	2.09	2.29	<0.001	3.88	0.34	0.032	0.84	0.003	0.072	0.024	0.016	0.022
Y	<0.03	3.26	1.00	0.72	0.67	<0.002	1.16	0.13	0.016	0.26	0.019	0.41	0.10	0.064	0.10
Zr	0.32	3.31	1.28	1.10	0.70	0.088	0.73	0.31	0.25	0.22	0.089	0.28	0.17	0.17	0.046
Nb	0.321	4.50	1.56	1.36	0.89	0.17	3.46	1.57	1.11	1.15	1.83	4.33	3.25	3.17	0.71
Mo	<0.001	5.67	0.45	0.19	0.96	0.042	0.19	0.13	0.12	0.036	<0.011	0.26	0.16	0.15	0.053
Sn	5.26	21.6	12.3	11.4	4.63	5.94	10.3	7.71	7.66	0.92	13.7	15.7	14.7	14.7	0.44
Sb	0.16	1.47	0.47	0.39	0.31	<0.032	0.22	0.062	0.056	0.035	<0.035	0.086	0.046	0.045	0.013
Ba	<0.001	35.5	7.47	1.16	9.31	<0.001	2.07	0.27	0.028	0.51	<0.001	0.39	0.089	0.029	0.11
La	0.06	45.7	7.60	2.93	10.8	<0.001	1.00	0.079	0.014	0.19	0.002	0.58	0.15	0.056	0.18
Ce	0.11	40.7	7.41	3.73	9.15	0.001	1.75	0.15	0.025	0.35	0.012	1.33	0.32	0.16	0.34
Pr	<0.02	4.53	0.75	0.36	1.00	0.001	0.24	0.023	0.006	0.05	0.002	0.18	0.041	0.018	0.047
Nd	<0.13	8.15	1.77	0.96	1.94	0.003	1.19	0.12	0.029	0.25	<0.009	0.66	0.14	0.074	0.17
Sm	<0.001	1.22	0.25	0.18	0.22	0.006	0.29	0.035	0.018	0.06	<0.01	0.13	0.034	0.025	0.033
Eu	<0.001	0.75	0.11	0.066	0.13	0.002	0.21	0.018	0.006	0.041	<0.002	0.007	0.004	0.004	0.001
Gd	<0.001	1.03	0.25	0.17	0.18	<0.008	0.31	0.041	0.023	0.065	<0.01	0.10	0.025	0.021	0.021
Tb	<0.01	0.44	0.05	0.037	0.071	0.001	0.065	0.006	0.003	0.012	0.001	0.017	0.004	0.003	0.004
Dy	<0.06	0.81	0.32	0.26	0.20	<0.004	0.40	0.04	0.016	0.081	<0.006	0.094	0.022	0.015	0.023
Ho	<0.001	1.15	0.10	0.052	0.19	0.001	0.056	0.006	0.003	0.011	0.001	0.015	0.004	0.003	0.004
Er	<0.04	0.78	0.24	0.19	0.16	0.002	0.17	0.025	0.01	0.042	0.006	0.03	0.011	0.01	0.006
Tm	<0.001	0.50	0.06	0.042	0.081	0.001	0.023	0.004	0.003	0.005	0.001	0.008	0.003	0.002	0.002
Yb	<0.07	0.60	0.20	0.18	0.11	0.005	0.091	0.016	0.011	0.02	<0.005	0.051	0.013	0.011	0.011
Lu	<0.001	0.22	0.05	0.036	0.046	0.001	0.015	0.004	0.003	0.004	0.001	0.007	0.002	0.002	0.001
Hf	<0.001	0.97	0.14	0.054	0.17	<0.001	0.10	0.031	0.022	0.021	<0.001	0.045	0.017	0.013	0.011
Ta	<0.001	0.51	0.11	0.061	0.11	0.02	0.097	0.06	0.056	0.021	0.46	0.68	0.56	0.56	0.057
W	<0.001	2.80	0.59	0.34	0.60	<0.001	0.99	0.09	0.021	0.20	0.006	0.026	0.011	0.01	0.004
^{204}Pb	0.004	0.71	0.13	0.063	0.15	<0.006	0.18	0.02	0.014	0.032	<0.006	0.023	0.01	0.009	0.004
^{206}Pb	0.04	13.5	2.53	1.21	2.98	<0.003	3.14	0.18	0.02	0.58	<0.003	0.038	0.008	0.007	0.008
^{207}Pb	0.06	10.6	1.82	0.90	2.16	0.002	3.21	0.16	0.019	0.58	<0.003	0.028	0.007	0.006	0.005
^{208}Pb	0.06	26.6	4.62	2.17	5.75	<0.004	7.17	0.36	0.038	1.31	<0.004	0.049	0.013	0.011	0.011
∑Pb	0.22	51.4	9.11	4.46	11.0	0.016	13.7	0.72	0.11	2.5	0.02	0.12	0.038	0.035	0.022
Th	<0.05	31.9	4.44	2.44	5.69	0.001	1.99	0.15	0.013	0.39	0.002	0.28	0.042	0.018	0.065
U	0.08	92.2	6.00	1.25	16.9	<0.001	0.71	0.073	0.009	0.17	0.003	0.044	0.01	0.008	0.009

Summary statistics treat concentrations lying below their respective detection limit as that mdl value. Calcium values are omitted for ACD1.15 due to high background. Abbreviations: Min.−minimum; Max.−maximum; G.M.−geometric mean; S.D.−standard deviation; NA−not available.

Table A3. Nano-thermooxybarometric estimations based on magnetite and ilmenite pairs from STEM-EDX data.

Sample	trellis, ACD1.15									
oxide, wt%	Mt1	Ilm1	Mt2	Ilm1	Mt1	Ilm2	Mt2	Ilm2	Mt-mean	Ilm-mean
TiO_2	0.51	49.47	0.59	49.47	0.51	49.35	0.59	49.35	0.55	49.41
Al_2O_3	0.08	0.24	0.06	0.24	0.08	0.29	0.06	0.29	0.07	0.26
$FeO_{(Total)}$	98.17	46.73	98.10	46.73	98.17	46.82	98.10	46.82	98.13	46.77
MnO	0.87	3.31	0.87	3.31	0.87	3.25	0.87	3.25	0.87	3.28
MgO	0.23	<mdl	0.23	<mdl	0.23	0.01	0.23	0.01	0.23	0.01
ZnO	0.08	0.20	0.08	0.20	0.08	0.16	0.08	0.16	0.08	0.18
V_2O_3	0.06	0.05	0.07	0.05	0.06	0.12	0.07	0.12	0.07	0.08
Sum	100.00	100.00	100.00	100.00	100.00	100.00	100.00	100.00	100.00	100.00
APFU										
Ti	0.014	0.935	0.016	0.935	0.014	0.933	0.016	0.933	0.015	0.934
Al	0.003	0.007	0.002	0.007	0.003	0.008	0.002	0.008	0.003	0.008
Fe^{3+}	1.968	0.121	1.964	0.121	1.968	0.124	1.964	0.124	1.966	0.122
Fe^{2+}	0.973	0.861	0.975	0.861	0.973	0.860	0.975	0.860	0.974	0.861
Mn	0.027	0.070	0.026	0.070	0.027	0.069	0.026	0.069	0.026	0.070
Mg	0.012	0.000	0.012	0.000	0.012	0.000	0.012	0.000	0.012	0.000
Zn	0.002	0.004	0.002	0.004	0.002	0.003	0.002	0.003	0.002	0.003
V	0.002	0.001	0.002	0.001	0.002	0.002	0.002	0.002	0.002	0.002
Sum	3.000	2.000	3.000	2.000	3.000	2.000	3.000	2.000	3.000	2.000
Calc. Methods (Mol frac.)	Ulv	Ilm	Ulv	Ilm	Ulv	Ilm	Ulv	Ilm	Ulv	Ilm
Lindsley & Spencer (1982)	0.014	0.937	0.016	0.937	0.014	0.935	0.016	0.935	0.015	0.936
Stormer (1983)	0.013	0.937	0.015	0.937	0.013	0.936	0.015	0.936	0.014	0.936
Geothermobarometer by										
X'Ulv & X'Ilm from:	T, °C	$\log_{10}fO_2$	T, °C	$\log_{10}fO_2$	T, °C	$\log_{10}fO_2$	T, °C	$\log_{10}fO_2$	T, °C	$\log_{10}fO_2$
Lindsley & Spencer (1982)	562	-19.20	569	-19.07	564	-19.04	572	-18.91	567	-19.05
Stormer (1983)	560	-19.24	567	-19.11	562	-19.11	569	-18.99	564	-19.11
Mean	561	-19.22	568	-19.09	563	-19.08	570	-18.95	566	-19.08

Table A3. (cont.) Nano-thermooxybarometric estimations based on magnetite and ilmenite pairs from STEM-EDX data.

Sample	orbicular, ACD1-3									
oxide, wt%	Mt	Ilm1	Mt	Ilm2	Mt	Ilm3	Mt	Ilm5	Mt	Ilm-mean
TiO_2	0.06	51.12	0.06	50.30	0.06	50.37	0.06	50.57	0.06	50.57
Al_2O_3	0.51	0.21	0.51	0.20	0.51	0.12	0.51	0.17	0.51	0.17
$FeO_{(Total)}$	98.61	33.43	98.61	34.20	98.61	34.79	98.61	33.51	98.61	33.51
MnO	0.54	10.94	0.54	11.37	0.54	11.36	0.54	11.13	0.54	11.13
MgO	0.19	4.30	0.19	3.93	0.19	3.37	0.19	4.61	0.19	4.61
ZnO	NA	NA	NA	NA	NA	NA	NA	NA	NA	NA
V_2O_3	0.08	<mdl	0.08	<mdl	0.08	<mdl	0.08	<mdl	0.08	<mdl
Sum	100.00	100.00	100.00	100.00	100.00	100.00	100.00	100.00	100.00	100.00
APFU										
Ti	0.002	0.934	0.002	0.921	0.002	0.927	0.002	0.921	0.002	0.921
Al	0.022	0.006	0.022	0.006	0.022	0.003	0.022	0.005	0.022	0.005
Fe^{3+}	1.973	0.126	1.973	0.152	1.973	0.143	1.973	0.152	1.973	0.152
Fe^{2+}	0.975	0.553	0.975	0.544	0.975	0.569	0.975	0.527	0.975	0.527
Mn	0.016	0.225	0.016	0.234	0.016	0.235	0.016	0.228	0.016	0.228
Mg	0.010	0.156	0.010	0.143	0.010	0.123	0.010	0.167	0.010	0.167
Zn	NA	NA	NA	NA	NA	NA	NA	NA	NA	NA
V	0.002	0.000	0.002	0.000	0.002	0.000	0.002	0.000	0.002	0.000
Sum	3.000	2.000	3.000	2.000	3.000	2.000	3.000	2.000	3.000	2.000
Calc. methods (Mol frac.)	Ulv	Ilm	Ulv	Ilm	Ulv	Ilm	Ulv	Ilm	Ulv	Ilm
Lindsley & Spencer (1982)	0.002	0.919	0.002	0.901	0.002	0.907	0.002	0.901	0.002	0.901
Stormer (1983)	0.002	0.920	0.002	0.903	0.002	0.910	0.002	0.902	0.002	0.902
Geothermobarometer by										
X'Ulv & X'Ilm from	T, C	$\log_{10}fO_2$	T, C	$\log_{10}fO_2$	T, C	$\log_{10}fO_2$	T, C	$\log_{10}fO_2$	T, C	$\log_{10}fO_2$
Lindsley & Spencer (1982)	493	-19.41	507	-18.32	503	-18.64	507	-18.35	503	-18.65
Stormer (1983)	492	-19.47	505	-18.45	499	-18.88	506	-18.37	501	-18.77
Mean	492	-19.44	506	-18.38	501	-18.76	506	-18.36	502	-18.71

APFU calculations are based on totals of four and three oxygen atoms in magnetite and ilmenite, respectively, using the ILMAT spreadsheet of Lepage (2003, and references therein). Average temperature and log(fO_2) from thermooxybarometers of Lindsley and Spencer (1982), Stormer (1983), and calibrations of Andersen and Lindsley (1985). Note that Zn was not observed in the orbicular magnetite and it was therefore not included among the measured elements. Calculated results from touching pairs. Abbreviations: Mt−magnetite; Ilm−ilmenite; Ulv−ulvöspinel; NA−not analysed.

Additional references

Andersen, D.J., and Lindsley, D.H. (1985) New (and final!) model for the Ti-magnetite/ilmenite geothermometer and oxygen barometer. Abstract, AGU 1985 Spring Meet. Eos Transactions, 66, 416.

Canil, D., and Lacourse, T. (2020) Geothermometry using minor and trace elements in igneous and hydrothermal magnetite. Chemical Geology, 541, 119576. https://doi.org/10.1016/j.chemgeo.2020.119576

Courtney-Davies, L., Ciobanu, C.L., Verdugo-Ihl, M.R., Dmitrijeva, M., Cook, N.J., Ehrig, K., and Wade, B.P. (2019a) Hematite geochemistry and geochronology resolve genetic and temporal links among iron-oxide copper gold systems, Olympic Dam district, South Australia. Precambrian Research, 335, 105480. https://doi.org/10.1016/j.precamres.2019.105480

Donovan JJ, Singer JW, Armstrong JT (2016) A new EPMA method for fast trace element analysis in simple matrices. Am Mineral 101, 1839–1853. https://doi.org/10.2138/am-2016-5628

Lepage, L.D. (2003) ILMAT: an Excel worksheet for ilmenite–magnetite geothermometry and geobarometry. Computers and Geosciences 29, 673–678. https://doi.org/10.1016/S0098-3004(03)00042-6

Lindsley, D.H., and Spencer, K.J. (1982) Fe−Ti oxide geothermometry: Reducing analyses of coexisting Ti-magnetite (Mt) and ilmenite (Ilm). Transactions, American Geophysical Union 63, 471.

Stormer, J.C. (1983) The effects of recalculation on estimates of temperature and oxygen fugacity from analyses of multicomponent iron-titanium oxides. American Mineralogist, 68, 586–594.

van Achterbergh, E., Ryan, C.G., Jackson, S.E., and Griffin, W.L. (2001) Data reduction software for LA-ICP-MS, in: Sylvester, P.J. (Ed.), Laser-Ablation-ICPMS in the Earth Sciences; Principles and Applications. Mineralogical Association of Canada, Short Course Series, 29. pp. 239–243.